Title
Enhanced performance of counter flow SOFC with partial internal reformation

Journal
International Journal of Hydrogen Energy, 39(34)

ISSN
0360-3199

Authors
Fardadi, Mahshid
McLarty, Dustin F
Brouwer, Jacob
et al.

Publication Date
2014-11-01

DOI
10.1016/j.ijhydene.2014.09.148

Available online at www.sciencedirect.com

ScienceDirect

journal homepage: www.elsevier.com/locate/he

Enhanced performance of counter flow SOFC with partial internal reformation

*Mahshid Fardadi, Dustin F. McLarty, Jacob Brouwer, Faryar Jabbari**

Department of Mechanical and Aerospace Engineering, University of California, Irvine, CA, 92697, United States

ARTICLE INFO

Article history:
Received 19 September 2014
Accepted 26 September 2014
Available online 22 October 2014

Keywords:
Solid oxide fuel cell
Partial internal reformation
Counter flow design
Thermal management

ABSTRACT

We study a counter-flow solid oxide fuel cell system and consider the challenges faced in minimizing thermal variations from the nominal operating conditions for a reasonable range of power tracking. Blower dynamics, reformer transport delays, spatial distribution of the heat generated and the resulting thermal response are among the issues considered. A novel approach, relying on partial internal reformation of the feedstock is proposed as a remedy to maintain a strong level of power tracking with minimal thermal stress to the fuel cell.

Introduction

The emerging distributed generation paradigm requires high efficiency, flexible and environmentally benign energy sources that can be installed at a variety of scales. Solid Oxide Fuel Cells (SOFC) are receiving increasing attention due to their high efficiency, low pollutant emissions, and scalability. The underlying electrochemical processes in the fuel cell occur at rates that can address all typical power tracking needs. There are, however, technical challenges that are faced at the system level. For example, reliance on external reformation results in transport delays in the reformer that can lead to fuel starvation or loss of power tracking ability. On the other hand, exclusive reliance on internal reformation leads to excessive thermal gradients due to disparate rates of electrochemical and reforming reactions at the same temperature. More generally, rapid changes in the power setting can result in excessive temperature spatial and temporal variations, with the commensurate increased thermal stress and possible reductions in durability and life of the fuel cell.

In Refs. [1–5] advantages of centralized controller for transient operation of SOFC are shown. In an earlier paper [3], we have studied power tracking and thermal control of a co-flow SOFC. The airflow rate (cathode inlet) and its temperature were shown to be effective actuators for thermal management. In Fardadi et al. [3], it was shown that a centralized controller offers important advantages for the co-flow design. Then an advanced control technique was used to minimize thermal variations, from nominal operating conditions, for a significant range of power variations. While these results were obtained under the assumption of perfect actuator mechanisms, subsequent work presented in Fardadi et al. [4,5] showed certain actuator limitations do not provide a significant challenge and can be addressed with relative ease. For example, the challenges associated with the parasitic power losses in the blower can be addressed by incorporating a model of the blower in the dynamic model and letting the controller balance the power needs of the blower.

* *Corresponding author*. Tel.: +1 949 824 6433; fax: +1 949 824 8585.
E-mail address: fjabbari@uci.edu (F. Jabbari).
http://dx.doi.org/10.1016/j.ijhydene.2014.09.148

The key actuator challenge identified in Fardadi et al. [4,5] was associated with fuel processing. The delays associated with fuel processing limit the ability of the fuel cell to provide power tracking. Since the transport delay in fuel delivery is slower than the electrochemistry dynamics, when power demand is increased the potential for fuel starvation and cell damage increases as well [7–9].

In Refs. [4,5], transport delays due to external reformation were handled by relying on internal reformation for a portion of the fuel used. The amount of this directly injected (into the anode) methane was used to adjust the overall fuel delivery, given the power demand. As a result, the external reformer is used at steady operating conditions and transport delays are avoided. Also, the use of a central controller that includes the model of the blower and a spatially resolved SOFC model were shown to provide a high degree of thermal control, keeping thermal variations from the nominal profile low (e.g., a few degrees for ± 15% step change in power).

Here, we focus on the counter-flow design for the SOFC. This configuration is the subject of interest due to its potential for higher efficiency due to higher utilization of electrochemically generated heat for fuel processing [10,11]. Counter flow configuration is more efficient because the anode entrance region will always have the highest current due to the reactant concentration, and in the co-flow this high current area occurs at the low temperature cathode inlet where Ohmic losses are higher than in the high temperature cathode outlet region. The higher efficiency comes at the cost of more challenging temperature distributions in the fuel cell and more challenging thermal control as the actuation mechanisms (e.g., cathode air flow rate and its temperature) are applied downstream, far from the most electrochemically active sites in which the majority of the heat is generated. This leads to several challenges, which are discussed and addressed in the rest of this paper. 'Dome'-like thermal profiles are caused by reformation cooling that dominates on one side of the fuel cell and cathode air cooling that dominates on the other side of the fuel cell. The 'dome' like thermal profiles lead to the need for a more detailed information regarding the thermal profile, which requires a spatial model (hence higher order models) to resolve in simulations, and a larger number of sensors in application of controls.

While partial internal reformation can again be used for enhanced power tracking, it often results in excessive thermal temporal variations and spatial gradients which can cause thermal stress. The solution provided here allows slow changes in the operation of the reformer to avoid excessive thermal gradients. This, in turn, requires a dynamic and spatially resolved model for the reformer to study the influence of the reformer transients and a feedback loop to adjust the amount of internal reformation in response to the reformer dynamics. Overall, it is shown that the proposed approach can be used for enhanced power following of counter flow SOFC technology, with minimal thermal stress and potential fatigue or damage, as shown in Results Section.

Background

Aguiar et al. [11,12] developed a dynamical model of an anode-supported intermediate temperature direct internal reforming (DIR) planar SOFC stack for both co-flow and counter-flow arrangements without considering inherent coupling between balance of plant dynamics and the fuel cell. Their main focus is on analyzing the electrochemical performance of the cell for different temperatures and fuel utilizations. They identified that both the fuel and air must be manipulated to maintain fuel cell operating condition during transients, though they were not concerned with controlling (or minimizing) temperature variations due to the fuel cell dynamics. In this paper, nominal temperatures remained unchanged in order to minimize overall temperature variation spatially and temporally.

Shaffer and Brouwer [13] developed a quasi-2-dimensional dynamic model of a direct internal reformation planar SOFC (DIR-SOFC) for counter-flow configuration to investigate effects of various parameters and assumptions on the temperature gradients across the cell. Results showed that positive electrode – electrolyte – negative electrode (PEN) temperature gradients will increase by improving the cell electrochemical performance, and manufacturing larger size cells. Shaffer and Brouwer conclude that by implementing effective controllers and by designing the stack with specific features, it may be possible to alleviate PEN temperature gradients. The work of Shaffer and Brouwer [13] and also that of Mueller [14] are the most closely related modeling methodologies to the one used in this paper. The model development for this control work was conducted in MATLAB Simulink® in order to take advantage of the built-in control tools.

Fuel cell stack

The current model is developed based on conservation of mass, species, and energy, as well as equations of convective and conductive heat transfer, steam reformation reactions and fuel cell electrochemistry. For spatial and temporal resolution, the fuel cell is quasi-dimensionally discretized (in 2-D) into nodes along the flow direction with each node consisting of four control volumes: PEN tri-layer, interconnect plate, anode, and cathode gas channel control volumes as shown in Fig. 1. Here the same methodology as Fardadi et al. [3–6] has been used to develop a dynamic model for an anode-

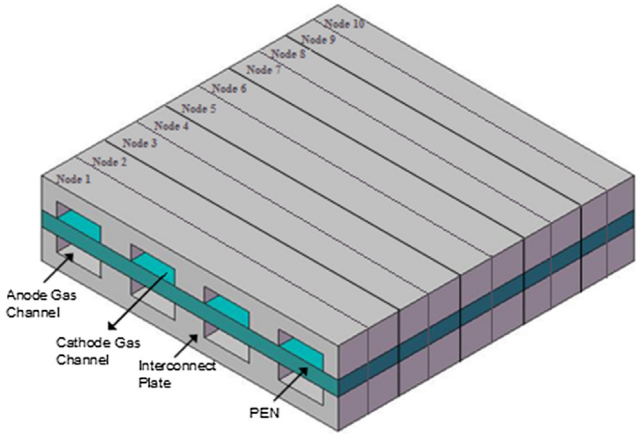

Fig. 1 – Quasi 2-dimensional counter-flow SOFC spatial discretization [6].

supported counter-flow configuration model. Only the physical and chemical processes that affect the timescale of interest (i.e., greater than 10 ms) are modeled. This includes the reformation kinetics, heat transfer and bulk channel flow. The electrochemical kinetics are assumed to be sufficiently quick to be considered always at steady state. The resulting dynamic model resolves the temperatures for the current collector plate, cathode gas stream, PEN assembly, and anode gas stream, local concentrations of six species within the anode (nitrogen, steam, methane, hydrogen, carbon monoxide and carbon dioxide), as well as oxygen and nitrogen within the cathode for a total of 12 states within each node (discretized length of the cell in the flow channel direction).

The external reformer processes the bulk of the methane and steam into hydrogen and carbon monoxide/dioxide, with a small portion of unreformed methane directly entering anode channels. Direct injection of methane, for addressing power following, increases the methane concentration entering the anode while simultaneously increasing the steam content. As a result, reformer kinetics are considered within the anode channels of the model in addition to the external reformer Important differences arise in the thermal profile due to the underlying endothermic reforming process which cools down the region near the fuel inlet, as shown further below.

Because the injected methane is primarily reformed near the inlet of anode, the counter-flow model has a more pronounced temperature 'dome,' as discussed above, and thus requires a more refined spatial discretization to capture the key characteristics for comparison with the previously analyzed co-flow configuration. The counter-flow model thus contains a larger number of states (higher order model) than the previous co-flow model. The granularity needed for this approximation has been studied along the lines used in Ref. [6], indicating that 10 nodes are sufficient (5 were sufficient in co-flow arrangements). If, we use 10 nodes, then in total the fuel cell is discretized into 40 control volumes (4 control volumes per node times 10 nodes in flow direction). The repeat cell unit is modeled with a periodic boundary condition to account for heat transfer between the modeled cell and adjacent cells in the fuel cell stack. The model here is developed based upon the same methodology that was used in Refs. [3–6] for co-flow and in Ref. [13] for counter-flow configuration, and the interested reader can consult these references for further technical details. The methodology used here has been previously used by others, including [14–26], who have compared predictions to both cell and system level experimental data [20,22–26]. The modeling methodology used here has been verified experimentally and used for controls development in previous work [27–33].

Blower

Cathode flow provides the bulk of the stack cooling and is responsible for maintaining fuel cell temperature. Internal heat generation changes with stack power output and fuel flow, and cathode flow must respond quickly to maintain a steady temperature profile during transient operations. A low temperature blower supplies the cathode air flow. Cathode flow transients are caused by blower dynamics, due to the rotational inertia, and by air mass storage, due to changing density with pressure in the relatively large volume of air manifold plumbing. The outlet pressure (p_{out}) and flow rate ($\dot{N}$) of the blower are assumed to be linearly proportional to the blower shaft speed [4,5]. The shaft speed is determined from a dynamic shaft torque balance defined in Equation (1) [4,5,14,34]. The impeller power (loss) is determined from Equation (2).

$$Jw\frac{dw}{dt} = P_{Blower} + P_{Impeller} \tag{1}$$

$$P_{Impeller} = -\frac{1}{\eta_{Blower}}\frac{\gamma RT_{amb}}{\gamma - 1}\left[\left(\frac{p_{out}}{p_{amb}}\right)^{\frac{\gamma-1}{\gamma}} - 1\right] \tag{2}$$

In these expressions R represents the gas constant, J is the blower rotational moment of inertia, P_{motor} represents power supplied by the controller, $P_{Impeller}$ represents the work transferred to the cathode inlet stream, η_{Blower} represents the isentropic compression efficiency (85%), and γ represents the specific heat ratio of air. Shaft speed is measured and provides an additional sensor to the controller.

External fuel processing (reformer)

The proposed approach here required a detailed reformer model to capture the fuel reformation transients. The reformer is discretized in a manner that is similar to that used for the fuel cell stack. A single planar repeat unit of the reformer reactor described by three control volumes is divided into 20 segments (nodes) in the primary flow direction. A hot gas channel, a catalyst coated solid plate and cold gas channel comprise the three control volumes of each node. The effective area of reformation is scaled by increasing or decreasing the number of repeating planar units. McLarty [34] showed that 20 nodes are sufficient to capture all of the physical behavior and the impacts of additional discretization beyond this, is minimal. Cathode exhaust is directed into the hot channels to provide the thermal energy necessary to balance the endothermic reformation of incoming fuel occurring within the cold gas channels. The solid plate conducts heat from the hot channels to the reforming fuel-water mixture, supports the reforming catalyst, and introduces a thermal mass that produces a thermal storage transient. The inlet properties to each control volume are species mole fractions, temperatures, and flow rates from the upstream control volume or the inlet boundary condition. The exit properties of each control volume are determined from an energy balance of the heat transfer and reformation kinetics in that control volume.

The reforming and water–gas-shift reactions (Equations (3) and (4)) are described using the kinetics outlined by Drescher [35] and B.A. Haberman and J.B. Young [36] respectively.

$$\text{Reforming}: \quad CH_4 + H_2O \xrightarrow{R_{rf}} CO + 3H_2 \tag{3}$$

$$\text{Water} - \text{gas} - \text{shift}: \quad CO + H_2O \xrightarrow{R_{sf}} CO_2 + H_2 \tag{4}$$

In which R_{rf} and R_{sf} represent the forward catalyzed reaction rate constants for the reforming and water gas

shift reactions, respectively, and defined in Ref. [37] as follows:

$$R_{rf} = \frac{28.52 \cdot p_{CH_4} p_{H_2O} \cdot \exp\left(\frac{-11{,}000}{RT}\right)}{1 + 16.0 \cdot p_{CH_4} + 0.143 \cdot p_{H_2O} \cdot \exp\left(\frac{39{,}000}{RT}\right)} \cdot AV \quad (5)$$

$$R_{sf} = k_{sf}\left(p_{H_2O} p_{CO} - \frac{p_{H_2} p_{CO_2}}{K_{ps}}\right) \quad (6)$$

$$k_{sf} = 0.0171 \exp\left(-\frac{103191}{RT}\right) \quad (7)$$

$$K_{ps} = \frac{\chi_{H_2} \chi_{CO_2}}{\chi_{H_2O} \chi_{CO}} \quad (8)$$

where AV represents the active surface area to volume ratio, which is set to 5×10^5 [37]. For both internal and external reformation, steam is added to avoid damage to the fuel cell due to coking. In simulations here, a fixed ratio of 2:1 is used for the steam to carbon at the points when methane is introduced. The reformation process uses some of the steam, resulting in an SCR of 0.87 at the outlet of the reformer (here by carbon we mean the total carbon in CH_4, CO and CO_2). This ratio is increased along the flow as the fuel cell electrochemistry uses the hydrogen and generates H_2O. The steam to carbon ratio behavior and effects are further discussed in the result section (partial internal reformation subsection).

The reaction kinetics are sensitive to temperature, and as a result thermal management of the reformer is paramount to sustain sufficient hydrogen concentration at the anode inlet. The chemical kinetic model of Xu and Froment has been used in Ref. [5] and results were qualitatively similar to the results presented here. For the kinetic model of Xu and Froment the species variations were less sensitive to temperature variation compare to the ones we used here. We intentionally used the more sensitive model to monitor the effects of higher variations in the mole fractions in the overall behavior of the fuel cell.

Model linearization and reduction for control

This section describes the linearization of the aforementioned spatially resolved dynamic model and evaluates the feasibility of applying the linear model in control systems development and evaluation. The procedure for linearization near a specific operating condition is described in Fardadi et al. [3,5]. For the controls development, the fuel cell model was linearized near its nominal operating condition as specified in Table 1 of the Appendix to this paper. The inlet temperature is specified to maintain an average electrolyte temperature of 800 °C with a temperature gradient of 10 °C/cm across a 10 cm length planar cell. The open loop response to a 15% load change differed by less than 1 °C between the reduced order linear model and the complete nonlinear system model. The resulting linear model takes the form of Equation (9) with the A, B_1, B_2, C_1, C_2, D_{11}, D_{12}, D_{21}, D_{22} matrices determined by the built-in Simulink tools.

$$\begin{cases} \dot{\delta x} = A\delta x + B_1\delta w + B_2\delta u \\ \delta z = C_1\delta x + D_{11}\delta w + D_{12}\delta u \\ \delta y = C_2\delta x + D_{21}\delta w + D_{22}\delta u \end{cases} \quad (9)$$

Here, $w(t) \in R^{m_1}$ is a vector of exogenous inputs (e.g., external disturbances and noise in the system), $u(t) \in R^{m_2}$ is the vector of control inputs, $z(t) \in R^{p_1}$ is a vector of control variables and $y(t) \in R^{p_2}$ is the measurement vector (sensors). Variables with δ denote change from the nominal (baseline) values.

The specific disturbances, actuators, and sensors are similar to those used for the co-flow configuration presented in Fardadi et al. [3–5] and listed in Table 2 of the Appendix. The control inputs of blower power and cathode inlet temperature are readily manipulated using an electric power controller and a bypass valve directing air past the inlet air heat exchangers. The objective of this work is to demonstrate the load following capability of an SOFC system while controlling PEN temperature variations, making fuel cell load the primary disturbance of interest and spatial PEN temperatures the control variables. The sensor selection was based upon practical considerations (ease of use via thermocouples etc.), proximity, and coupling with the key performance objective; reducing the temperature variations from the nominal profile along the fuel cell during transient operation. In the counter-flow configuration, a higher number of nodes is required to capture the more pronounced temperature dome profile, which results in a higher order model, compared to the co-flow case. Additionally, the large temperature gradients near the anode inlet where reforming rates are high require a higher number of sensors, as well, particularly near this key region.

Measurement of blower shaft speed provides an additional sensor capable of capturing the fast dynamics associated with the blower. Temperature measurements included are the anode outlet temperature, and interconnect, plate temperatures at various locations. Since PEN temperatures are not easily measurable, plate temperatures, which are in close proximity to the PEN and can more easily be measured, are used. We also use the cathode outlet temperature as it closely related with the overall thermal conditions of the anode inlet.

Fuel flow rate is linearly related to current which is an indirect measure of heat generation in the fuel cell. As a result, we used a measurement of the fuel flow rate as another sensed variable for the controller. Fuel flow rate is also required to use in a separate control loop to regulate the required CH_4 in the fixed ratio partial internal reformation scheme, which will be discussed in Partial internal reformation Section.

Model reduction

For the purpose of controller design, the blower model was integrated with fuel cell stack model. The full linearized model contains 122 states 10 fuel cell nodes with 6 anode species, 2 cathode species, and 4 temperatures (anode, cathode, PEN, plate). The final two states represent the blower. A reduction in the number of states will reduce computational burden and sensitivity to numerical error. The model is reduced to 99 states by removing the uncontrollable and unobservable states. Further state reduction is conducted by calculating the Hankel singular values [38] of the system, and keeping only those states with singular values greater than 10^{-2}. The resulting model has 23 states. The open-loop

response to the same 15% load transient remained within 1 °C of the full order linear model. Since these results follow Fardadi et al. [3,5], details are omitted for brevity.

Feedback control design

The control design uses the H-infinity approach and the LMI toolbox of MATLAB [40], which was previously applied in Fardadi et al. [4]. The goal is to minimize fuel cell temperature variations from the nominal operating conditions. The reduced order linear plant model is applied to obtain a compensator in the form of Equation (10).

$$\begin{cases} \dot{x}_c = A_c x_c + B_c \delta y \\ \delta u = C_c x_c + D_c \delta y \end{cases} \quad (10)$$

The controller structure in Fig. 2 is aimed at minimizing the effects of disturbance, e.g., power demand, on the fuel cell temperature variations from the nominal case. In Fig. 2, the box 'Plant' refers to the actual nonlinear model, which is a blower model and a reformer model integrated with the fuel cell model, and valves. The nominal values of all variables u_{ref}, y_{ref}, w_{ref}, and z_{ref} are found from steady state conditions specified in Table 2. The disturbance δz represents spatial temperature variation from nominal, which is defined as $\delta z = z - z_{ref}$. Similarly, a load variation is represented by δw which results in a change in the operating conditions from the steady state, i.e. δy. The resulting, δy, pass through the controller, which specifies the inputs (δu) such that δz is minimized. The controller has the same order as the plant (i.e., dim of A_c is the same as dim of A). Technical details are omitted for sake of brevity but an interested reader can consult references [38–42] for details.

Results

The primary actuators used for fuel cell system control (blower power, cathode inlet temperature, and fuel flow) all experience some degree of delay. Fardadi et al. [4] showed that incorporating the blower dynamics into the model when developing a central controller can eliminate the 'non-minimum phase' behavior often associated with the neglected blower dynamics. The thermal inertia in the heat exchanger may lead to a thermal transport delay when controlling for the cathode inlet temperature. Fardadi et al. [4] demonstrated that thermal transport delays between 5 and 20 s do not significantly affect fuel cell thermal transients. The delays in fuel reformer introduce delays into the fuel delivery on the order of 1–5 s, which can significantly diminish power tracking capability. This section presents results of dynamic simulations of load following operation with these non-ideal actuators. The simulations were conducted with the spatially resolved model of a counter-flow SOFC with the reduced-order linear control developed in the previous section. Two system integration concepts are considered; 1) complete external fuel processing, 2) partial internal fuel processing.

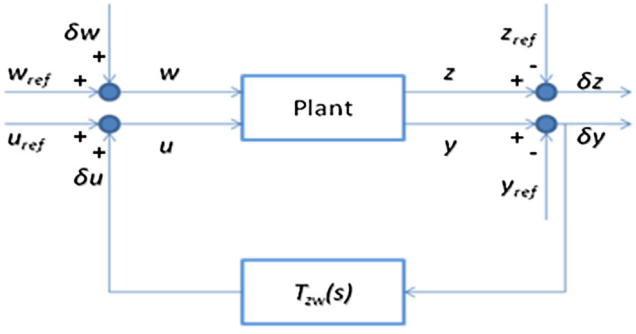

Fig. 2 – Feedback control block diagram.

The non-ideal actuation mechanisms introduce similar behavior to the counter-flow SOFC system as was seen in the co-flow case. The cathode pre-heat bypass delay is the most benign, resulting in relatively small overshoot/undershoot in fuel cell temperatures in response to step increase and decrease perturbations of 15%. The fuel transport and processing delay can lead to fuel starvation and consequently high cell stress for conditions of fast power tracking. The valve actuation and fuel processing delays are assumed to be unknown during control development. Thus, the controller will inevitably be faced with unanticipated errors that are not included in the model for controller design purposes. System performance is degraded by imperfect actuators in the form of increased internal temperature variation and decreased power tracking. Thermal variations that result primarily from the blower dynamics can induce cell thermal stress leading to fatigue or failure. Decreased power tracking that is the inevitable result of fuel processing delay, increases the dynamics which the grid power must accommodate or increases the size of an accompanying battery required in a stand-alone or micro-grid application.

The FC operating power set-point is the algebraic sum of the output power demand and the blower power determined by the controller. The delivered power is thus the generated power minus the blower power as specified in Equation (11) where y_c is blower power demand (controller command), y_s is the system power actually supplied and y_{fc} is FC power produced.

$$y_s = y_{fc} - y_c \quad (11)$$

If the blower power demand is met precisely, perfect power following may not be possible. Such a situation can occur when fuel cell power cannot be raised fast enough (e.g., when experiencing reforming delays) or when the reference power of the fuel cell reaches the maximum allowable power. Partial internal reformation Section discusses the utilization of direct injection of CH_4 to address this challenge.

External reformation transients

The most aggressive transient for a fuel cell to meet is a large step change. In the current simulation at 1000 s, an external power demand step decrease of 15% to 3 kW was applied followed by a step increase of 30% to 4 kW at 5000 s. Since thermal dynamics are fairly slow (due to the large SOFC thermal mass) 4000 s are required for the open loop temperature variations to reach steady state for significant applied perturbations.

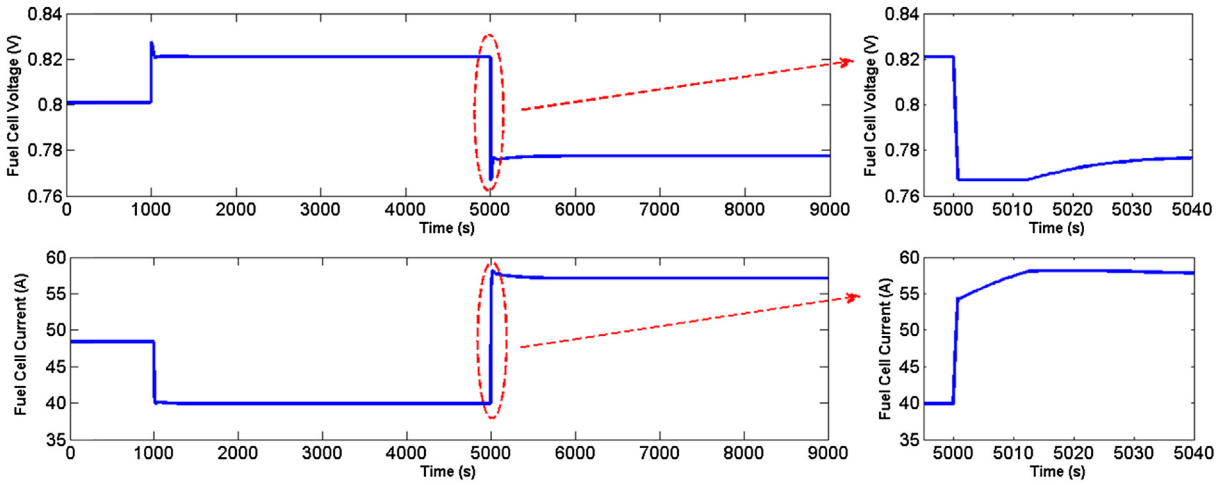

Fig. 3 – Predicted fuel cell voltage and current during transient.

Fig. 3 presents the results for system response a 33% step change perturbation from 3 kW to 4 kW. The electrochemistry responds instantaneously with a reduction in voltage and a corresponding increase in current. Due to the fuel processing delay, increasing current without the required fuel results in increased fuel utilization. When the current increases faster than the fuel transport, rapid changes in the voltage can occur and fuel starvation is possible. At fuel utilizations above 95% the anode electrode can be rapidly and permanently oxidized, resulting in permanent stack damage [33,43–45]. As a safety measure, the controller imposes a lower limit of 0.77 V for the voltage, which corresponds to 94% fuel utilization, to prevent fuel starvation. The inset charts illustrate how, at 5000 s, current rapidly increases to 55 amps when the voltage safety limit engages. Subsequently the current continues to increase at a slower rate corresponding to the fuel transport delay. After the power set-point is reached at 5012 s the fuel increase catches up with the current increase and fuel utilization settles at 85%. The additional fuel changes the current–voltage relationship and raises voltage to nearly 0.78 V.

As power increases, so too does the fuel flow rate through the reformer. This results in substantial changes in the reformation chemistry (e.g., partial fraction of the hydrogen in the reformer outlet – anode inlet) and anode inlet temperature, which in turn it may affect fuel cell performance (more on this later).

Fig. 4 shows variations in anode inlet temperature during these transients. Here a worst case scenario has been simulated by directly coupling a reformer model without independent temperature control. The closed loop integration of the fuel cell and reformer can cause undesirable transient response. If the cathode exhaust is cooled during a transient, the heat delivered to the reformer is less, and the fuel composition supplied to the FC will contain more CH_4. Typically, the thermal mass of the reformer and the relative excess of thermal energy available in the cathode exhaust are sufficient to accommodate most transients, but, any substantial

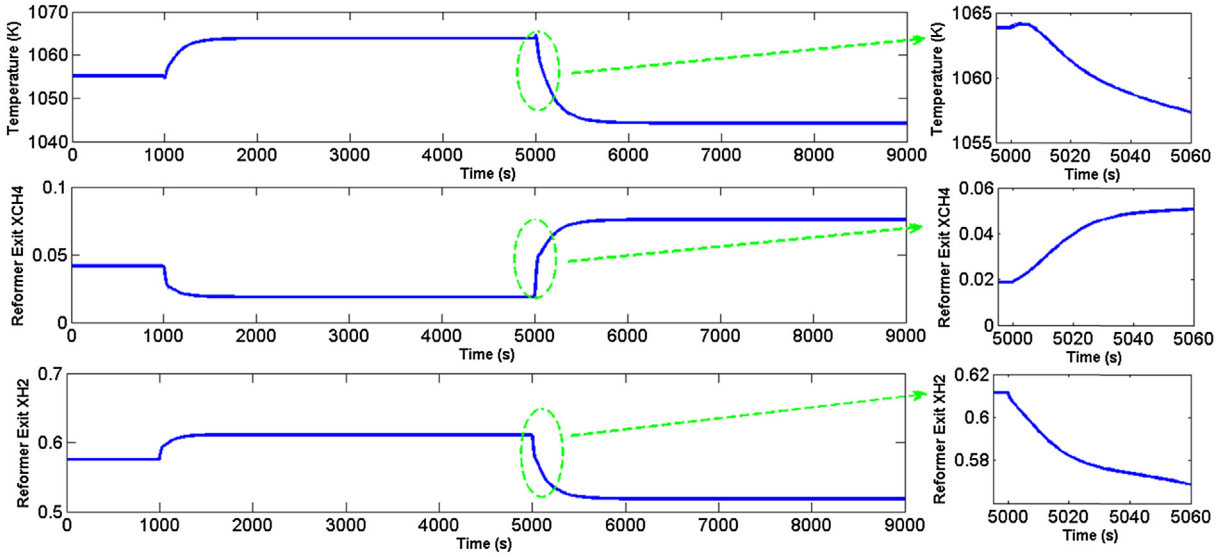

Fig. 4 – Predicted anode inlet temperature and change of species concentration at reformer outlet under load perturbation.

delay in the fuel mass transport (delivery to the reformer) is an example of a transient that is not easily overcome by the thermal inertia of the reformer.

The top chart in Fig. 4 illustrates the anode inlet temperature variation during the same step-change simulation. A rapid increase in power introduces additional fuel to the reformer before any additional heat has been generated in the FC. This leads to a reduction in reformer temperature, and therefore anode inlet temperature. The ±10° temperature variation is tolerable given the high operating temperatures and the fact that the fuel cell typically operates with 100 °C temperature variation from inlet to outlet.

The two bottom charts of Fig. 4 illustrate the change in hydrogen and methane concentration leaving the reformer as it is cools during this transient. Hydrogen concentration is reduced from 61% to 52% while the methane content quadruples to nearly 8%. This fuel will be quickly reformed in the FC anode and can lead to steep local temperature gradients near the fuel entrance. It is possible to incorporate independent temperature control of the reformer into the SOFC system design to mitigate these concentration variations. While the reformer is sensitive to temperature variations as noted above, such a variation is typically slow due to the relatively large reformer thermal mass, and in the current case transient thermal responses typically take >500 s. The variations in inlet anode mole fractions did not significantly alter the overall SOFC performance.

Fuel processing delay

The fuel processing delay referred to previously is illustrated in Fig. 5. The delay can be seen as the difference between the fuel demand (blue line) and fuel supply (dashed red line). It takes nearly 30 s for the external reformer to meet the fuel demand due to transport delay [7–9].

Fig. 6 and Fig. 7 show fuel cell's PEN temperature variation under ±15% load perturbation for both open loop (Fig. 6) and under feedback control (Fig. 7). Open loop PEN temperature variation is between 11 K and 45 K from nominal operating conditions in response to the increasing power step change perturbation, depending upon the node considered (i.e., location along the length of the cell). Fig. 7 shows that the controller is capable of maintaining the maximum temperature variation to within 7 K from nominal conditions, which is a satisfactory result.

Fig. 8 shows the power following profile for ±15% step changes in power demand from nominal operating conditions. During the step change from 85% to 115% of nominal power there is a significant gap between the net power produced and system power demand. The power tracking error reaches 6% and persists for 12 s. Recall that the fuel processing delay introduced by the external reformer has a time scale of approximately 15 s. The power can recover before the fuel flow is completely recovered, albeit at a higher fuel utilization. After 15 s the fuel flow reaches steady-state and fuel utilization normalizes to the desired 85%.

These results, coupled with the insight that small variations in inlet fuel composition during transients have little effect on stack performance, lead to the justification for direct fuel injection into the anode during step-load response. To avoid the power tracking error caused by the fuel processing delay the supplemental fuel needed during a step increase in power demand perturbation will be provided directly to the stack, bypassing the external reformer as in Refs. [4,5].

Partial internal reformation

In the previous section, we showed that the fuel processing delay in the reformer causes significant problems in power following. In this section we will discuss partial internal

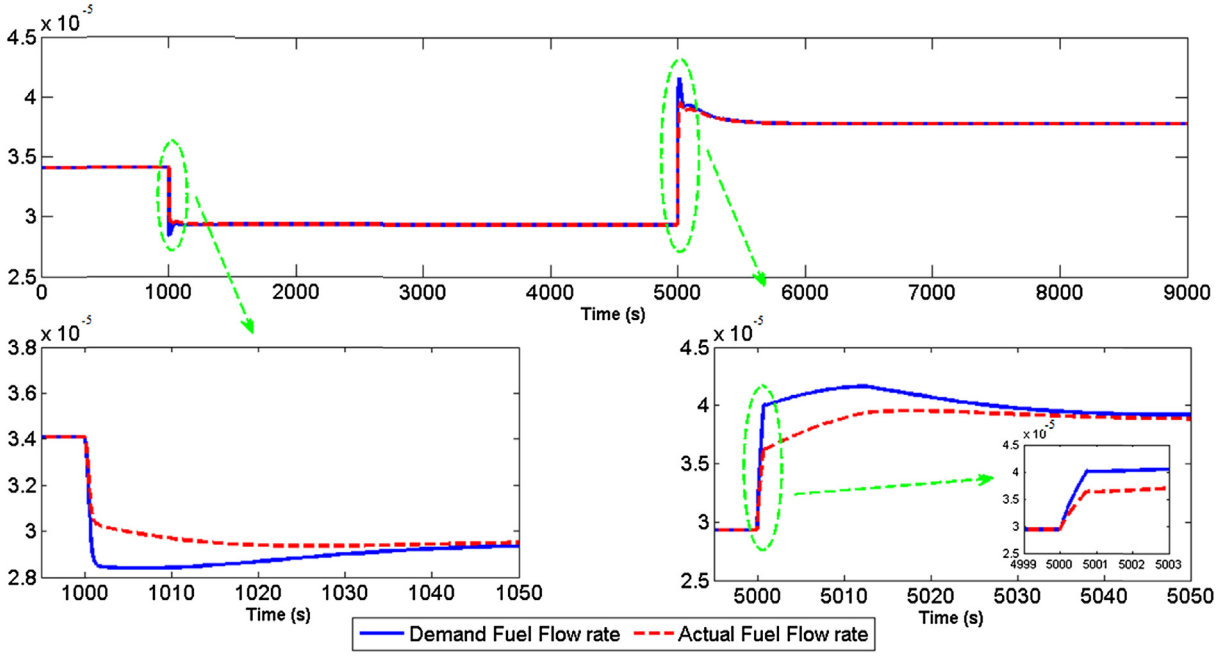

Fig. 5 – Predicted molar fuel flow rate.

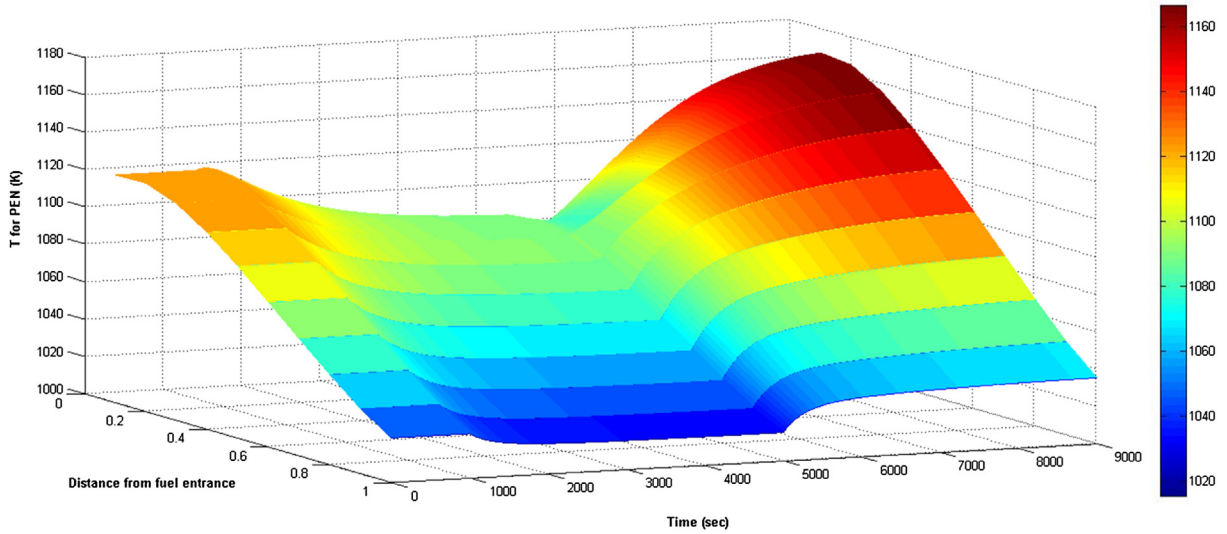

Fig. 6 – Predicted open loop temperature variations for Counter-flow configuration.

reformation, its advantages and disadvantages, as an alternative method. Similar to the co-flow case [4,5], initially we will use directly injected methane, for roughly 20% of the total fuel needed. For changes of up to about 15% in power, we then adjust the amount of methane to response to the changes in fuel demand, as the power drawn from the fuel cell is altered. As a result, the external reformer is allowed to operate at a steady condition and the delay and performance degradation of the reformer are avoided and replaced by the fast dynamics associated with valves that regulate the flow of methane. On the other hand, since most of the reformation is completed near the fuel entrance, internal reformation may result in excessive thermal gradients in this region. Higher blower power is required to suppress the higher overall thermal gradient for the co-flow configurations, thus reducing the overall system efficiency. For the performance measure, as in Refs. [4,5], we propose using the ratio of net power produced (i.e., for external use) to the fuel flow rate (fuel used) – see the Appendix for details.

In the co-flow case, partial internal reformation results in lower temperature variation for the case of open loop at the cost of a modest performance reduction of 1.5% compared to the case of 100% external reformation. This performance reduction is due to the need for higher inlet mass air flow and temperature at the cathode inlet to counter the cooling effects of extra methane introduced into the anode and reformed when power is increased.

For the counter-flow configuration, however, partial internal reformation leads to around a 5% increase in the performance measure compared to the case of 100% external reformation. This is due to the fact that, in the counter-flow case, cathode air cooling is introduced at the other end of the fuel cell and thus has less influence on the regions near the anode inlet, where the extra methane will be internally

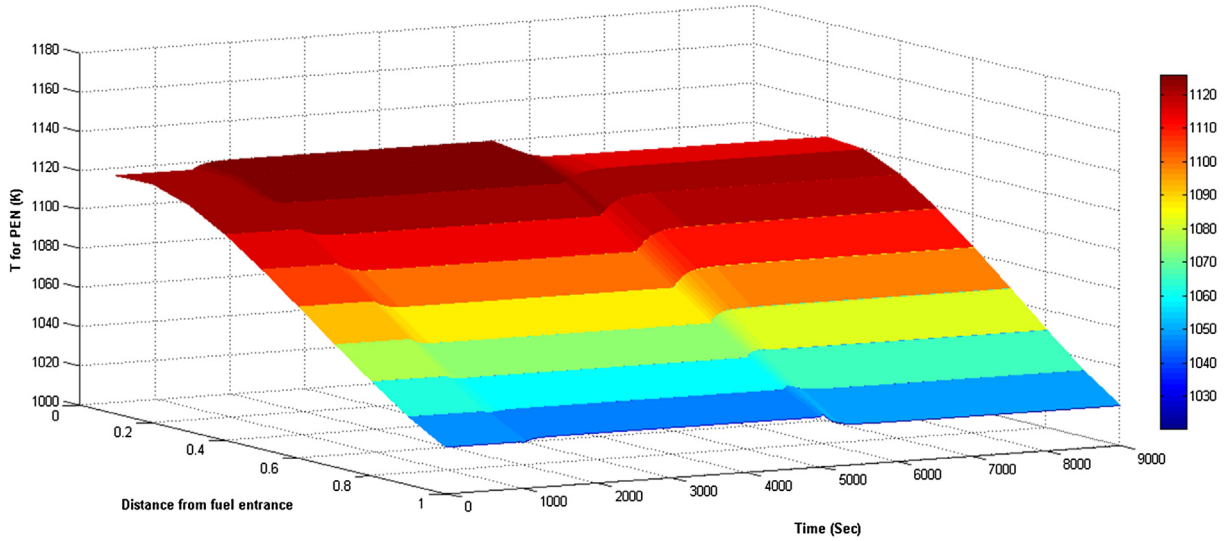

Fig. 7 – Predicted closed loop temperature variations for Counter-flow configuration.

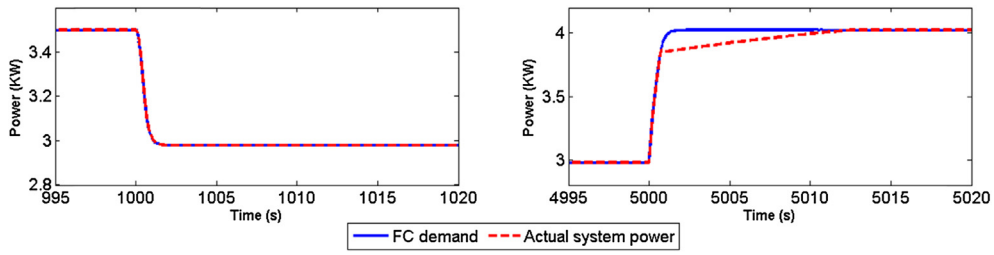

Fig. 8 – Predicted load Tracking profile.

reformed. As a result, the need to increase the temperature of the cathode air is obviated and lower air flow rates will be needed, leading to lower power usage by the blower, to keep the same 100° maximum temperature difference. One could use higher blower power to have less than 100° total temperature change and less steep temperature gradients, but for the sake of comparison with the co-flow case, here we kept the same 100° maximum temperature difference.

On the other hand, unlike the co-flow configuration, in counter-flow using a constant flow rate for external reformation can lead to larger temperature gradients. Once the power demand is increased, more methane is injected, which cools the anode inlet area. Due to an overall increase in the heat generated, more cooling will be provided by the actuation mechanism at the cathode inlet, leading to a more pronounced dome, and thus larger thermal gradients. Results associated with this phenomenon, including temperature profiles, and a possible remedy to deal with excessive gradients will be discussed next. To address this challenge, for counter-flow configuration a constant *ratio* of pre-reformed fuel to the direct injection of CH_4 has been tried. Such a fixed ratio prevents excessive dome-like gradients and yields a profile similar to the nominal one, leading to lower overall thermal gradients, as shown in the results section below.

Naturally, maintaining a fixed ratio requires concurrently manipulating the amount of external and internal reformation amounts, which might lead to the same delay related difficulties as experienced previously. To address this, we use methane injection during the transients to ensure proper fuel availability, then adjusting the methane injection to maintain the fixed ratio as the reformer flow rate reaches steady state. Given the duration of this transient, and the overall thermal mass of the fuel cell, this combination allows strong power tracking with reduced thermal variations. In the results below this approach and its impact on efficiency and the thermal profile will be discussed.

The operating conditions for a 5 kW fuel cell with partial internal reformation are listed in Table 3 in the Appendix. Recall that the inlet temperature is specified to maintain an average electrolyte temperature of 800 °C with a temperature gradient of 10 °C/cm across a 10 cm length planar cell. Note that the operating conditions here are somewhat different from the pure external reformation case discussed earlier. This difference is due to the use of different air flow and temperature to keep the same 100° maximum temperature difference between the air inlet and the dome of the profile.

Partial internal reformation leads to a higher performance measure due to the lower use of blower power to keep the same 100° maximum PEN temperature difference at nominal operating conditions. This is due to the fact that the endothermic internal reformation directly uses some of the heat generated by the electrochemistry; thus the fuel cell requires less air flow to keep the overall temperature the same. On the other hand, this comes at the expense of higher local temperature gradient especially near the fuel inlet where most of the internal reformation occurs.

To evaluate the closed loop results, given the large gradients near the anode inlet, we put more emphasis on temperature variations of the first node (by multiplying δT_1 by 2). Thus the closed loop temperature variation is a result of a controller that is designed for the modified controlled variable z. Result shows that the open loop PEN temperature variations are between 14 K and 35 K for increasing power and that the controller is capable of maintaining the temperature variation within 14 K from nominal condition during a ±15% power demand step perturbation. Although the cost function has been adjusted by modifying "z", temperature variation from nominal condition for the first node is still around 14 K. Without modifying the cost function the temperature variation from nominal condition for the first node is around 20 K.

These results imply that a constant flow rate of external reformation is not as beneficial as for the co-flow case and leads to an additional 10–15° temperature variation from nominal. This is due to the internal reformation that occurs near the anode inlet, but unlike the co-flow case, in counter-flow configuration the actuators are on the opposite side of the fuel cell and are thus not as effective in mitigating thermal variations.

The reliance on internal reformation discussed here provides the needed fuel with minimal delay. This, however, can alter the ratio of internal to external reformation, particularly during power increases, leading to a higher ratio of directly injected methane and thus excessive cooling near the anode inlet and higher thermal gradients. To counter this, the ratio is slowly restored to the nominal value.

Fig. 9 shows the schematic of the feedback loop used here to regulate the amount of directly injected CH_4. Here, $\dot{N}_{Total}$ is the total molar flow rate of fuel plus steam (ratio of 2:1 for steam to carbon) required for the fuel cell to provide the power demand, while $\dot{N}_{EXT}$ is the flow rate of pre-reformed fuel from the external reformer. The difference, $\dot{N}_{INT}$, is the flow rate of mixture of methane and steam introduced directly into the anode, this ratio, of 1/3 CH4 and 2/3 water is used to keep the

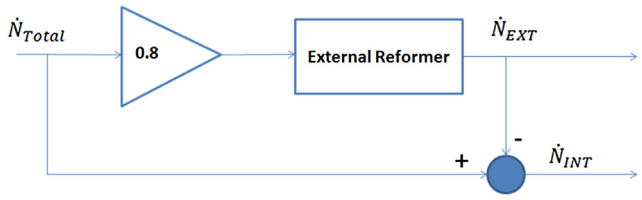

Fig. 9 – Partial internal reformation block diagram.

same steam to carbon ratio, sufficient to avoid carbon deposition [14,43–48].

Experimental studies have shown that no carbon deposition was observed for SCR higher than 1.5–1.6 (e.g. in an Ni-YSZ in an SOFC [48], see also [43–47]). It is worthwhile to note that the steam to carbon ratio in the fuel cell varies from 0.87 at the inlet to 3.46 at the outlet of fuel cell if there is no direct injection of the methane/steam discussed above. The additional mixture changes the profile: somewhat higher SCR throughout (e.g., 1.35 at the inlet and 3.6 at the outlet). Higher SCR can absorb some of the heat and result in somewhat more cooling at the inlet and lower voltages due to the higher partial pressures in the Nernst terms. For damage prevention, however, some steam is considered necessary. The values used here are consistent with what is considered safe (see Refs. [14,43–48]). The overall sensitivity of the fuel cell performance to the precise value of the SCR is limited. For example, for an SCR of 1.5 versus 2.5 for the fuel used, higher steam to carbon ratios resulted in slightly more loss in Nernst equation, which resulted in slightly lower voltages and higher currents (i.e. by the ratio of approximately 1/50—or 2% of the nominal values). The thermal profile however has a somewhat more pronounced change particularly in the case of partial internal reformation. There, the cooling near the entrance is more pronounced due to absorption of heat by cooler steam with somewhat higher temperatures near the exit due to the slightly higher loss terms (thus more heat generation). These are all within the same 2% of nominal values. The overall average temperature differs by 2° or less out of more than 1000 average temperature).

In steady state conditions, $\dot{N}_{EXT}$ and $\dot{N}_{INT}$ correspond to 80% and 20% of the needed fuel (see the Appendix for the relevant calculations). When power is increased, 80% of the required fuel flow rate enters the reformer. Due to the fuel processing delay the flow rate at the outlet of the reformer is less than 80% of the total flow rate for the duration of the delay and the flow rate of mixture of methane and steam calculated as:

$$\dot{N}_{INT} = \dot{N}_{Total} - \dot{N}_{EXT} \quad (12)$$

This approach is based upon the assumption that the variations in partial fractions of the fuel in the reformer outlet are relatively small during transients. Note that results in Figs. 5 to 8 showed that the variations in anode compartment mole fractions did not have a substantial effect on overall fuel cell performance.

The left chart on Fig. 10 shows the open loop steady state temperature profile for the three different cases of: (a) partial internal reformation at nominal operating conditions with 80% of fuel reformed externally, (b) 15% power demand step increase keeping the amount of external reformation fixed, and (c) 15% power demand step increase for a fixed ratio of external reformation to the total fuel used. Here, for the nominal conditions, we have 100° maximum temperature difference between the dome of the profile and the fuel inlet established as the nominal operating conditions.

Increasing power results in increasing fuel flow which results in decreasing anode inlet temperature (and some slower cooling effects on the reformer). Decreasing anode inlet temperature as well as higher amounts of internal reformation results in cooling the area near the anode inlet and higher temperature gradient in that area.

Comparing the three temperature profiles – in the open loop – shows that using a fixed amount of external reformation results in increasing temperature gradient near the anode inlet, which is due to the cooling effect of increased internal reformation on the area near the fuel entrance. On the other hand, using a fixed ratio of external to internal reformation results in a temperature profile similar to the nominal one and prevents excessive gradients at the expense of higher temperature variations from nominal conditions.

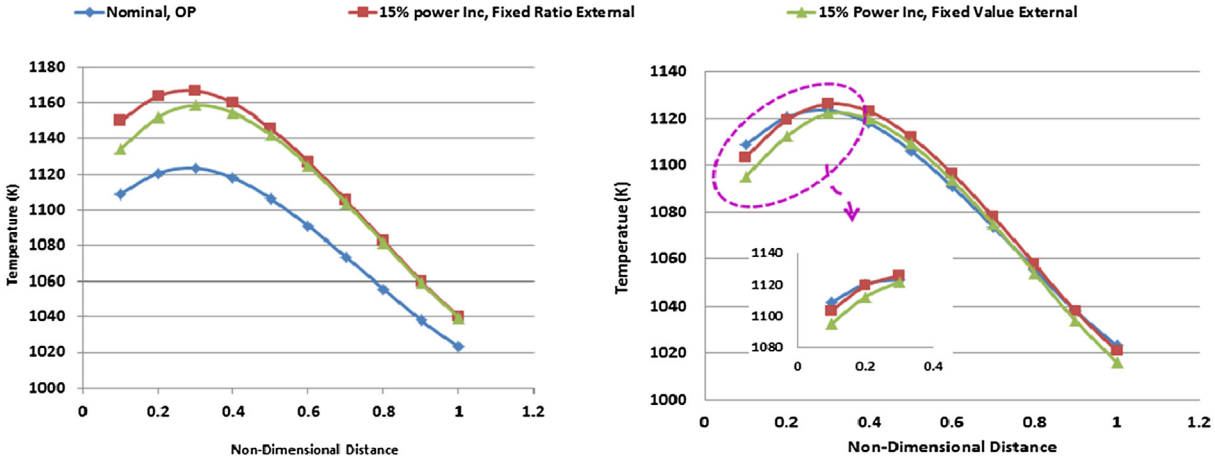

Fig. 10 – Predicted steady state temperature profile for partial internal reformation (left: open loop, right: closed loop).

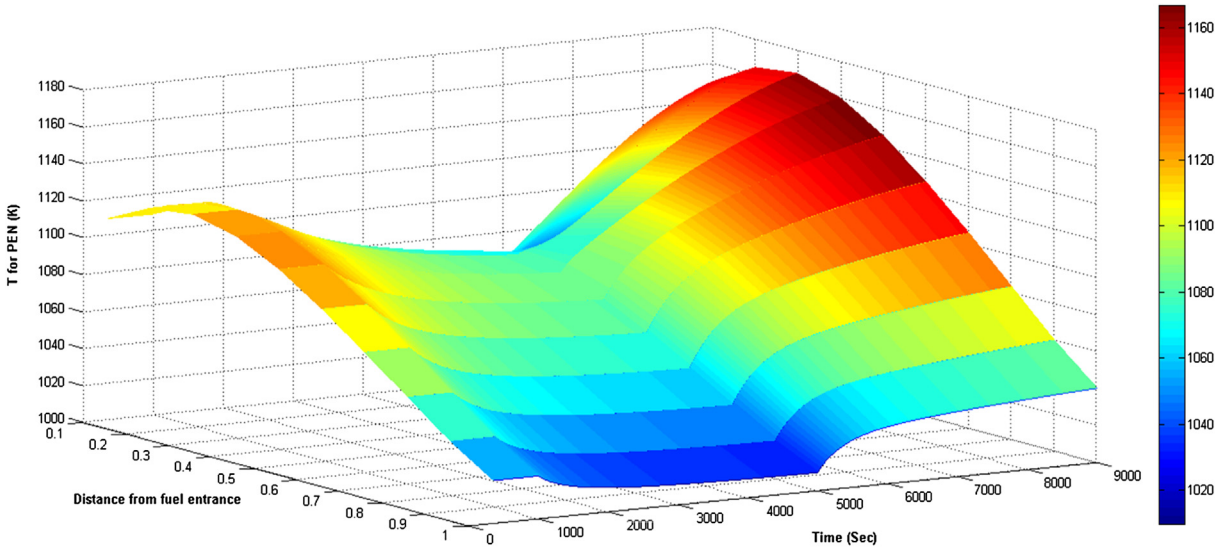

Fig. 11 – Predicted open loop temperature variations, fixed ratio of 80% external reformation at operating condition for counter-flow configuration.

The right chart on Fig. 10 shows the closed loop steady state temperature profile for the same three cases. The higher temperature gradient near the fuel entrance for fixed amount of pre-reformed fuel in open loop temperature profile results in higher temperature variations in the closed loop temperature profile as well. This is due to higher ratio of internal reformation (during transients as well as steady state) and having counter-balancing actuators at the opposite end of the fuel cell. The current controller aims to minimize the overall temperature variations from nominal conditions, which leads to lowering the entire temperature profile by increasing blower power and decreasing cathode inlet temperature. This would result in higher temperature variations near the fuel inlet for the fixed value external reformation case, compared with the fixed ratio case.

Figs. 11 and 12 show the results for the fixed ratio case: open loop temperature variation is between 19 K and 56 K for increasing power and controller is capable of maintaining the temperature variation within 8 K from nominal condition during a ±15% power demand step variation from nominal conditions. Of course, during transients the percentage of internal reformation will be temporarily more than 20% of the total flow rate, to ensure that there is enough fuel for power tracking. Due to the limited delay in reformer flow and the thermal masses involved, this does not result in significant additional thermal variations. As a

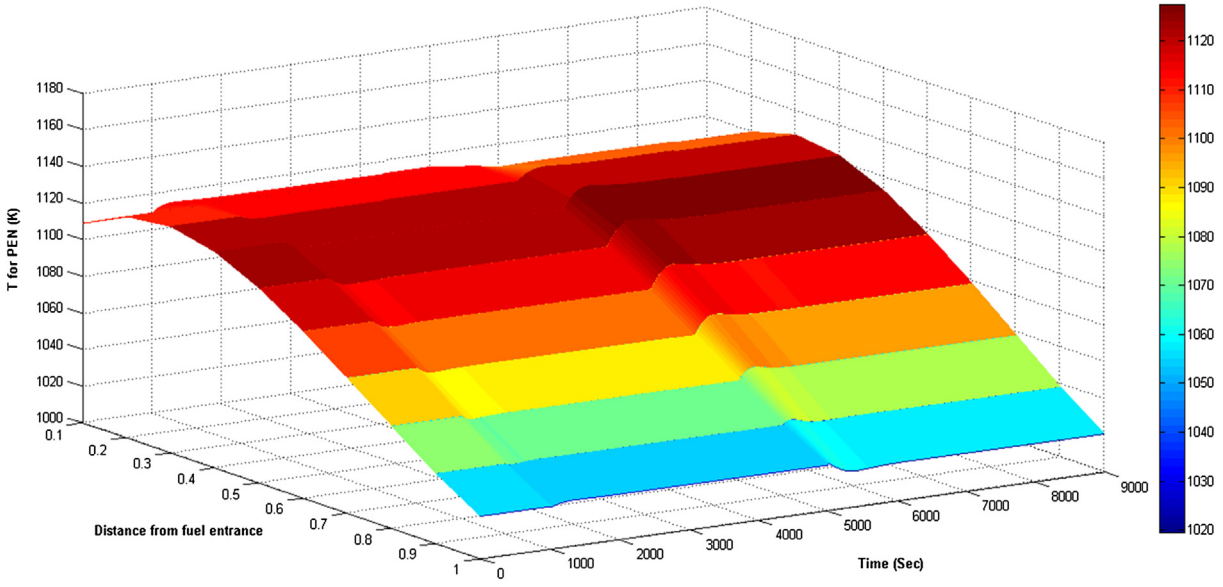

Fig. 12 – Predicted closed loop temperature variations, fixed ratio of 80% external reformation at operating condition for counter-flow configuration.

result, the higher efficiency of the partial internal reformation is maintained.

Once power is increased, more heat is generated which would require higher air flow rates in both co-flow and counter flow configurations to keep the temperature profile close to the nominal. To avoid excessive cooling at of the electrolyte assembly at the cathode inlet the recirculation or pre-heating must increase, leading to additional power losses. In counter flow the heat convected downstream of anode warms the cathode inlet (i.e, fuel outlet) preventing excessive cooling due to higher air flow rates. In co-flow, since the air and fuel enter from the same direction, cathode temperature is increased to avoid excessive cooling, which in turn requires higher air flow rates and blower power use. Similar results were obtained when steady-state optimization was used by Inui et al. [23]. This is an important contributor to the higher efficiencies in counter-flow fuel cells.

Fixed ratio partial internal reformation improves the power following ability of the fuel cell significantly and eliminates the gap that was seen in the external-reformation-only case. This is at the expense of higher temperature variations compared with the 100% external reformation case. Similar power tracking is obtained when a fixed amount of external reformation is used, albeit with somewhat higher temperature variations from nominal conditions.

Generally, the controllers used have significant tolerance with respect to changes in the operating conditions. For example, in Ref. [5] the controller designed for one reformation chemical kinetics was applied to an FC in which another reformation chemical kinetics was used. Similarly, in Ref. [4] the controller designed for external reformation set-up was applied to the case where partial internal reformation was used. Results were quite similar (variations on the order of 0.1 percent), confirming that the controller has a measure of robustness regarding operating conditions.

Conclusion

Transport delays in external reformation and thermal variations due to rapid power following are two of the most significant challenges in developing aggressive power tracking for fuel cells, the latter being an important component of thermal stress and fatigue that can reduce the durability and life of the fuel cell. The counter flow configuration is studied here. It is shown that partial internal reformation, in which a portion of the fuel is directly injected as methane into the anode, can be used to provide fast and reliable power following. Advanced control techniques are used to mitigate thermal variations. Unlike the co-flow configurations, in order to avoid excessive thermal gradients, the amount of externally reformed fuel is adjusted, slowly. This results in a different structure for the controller and fuel flows for maintaining temperature profiles during transient operation. Thus the controllers must respond in the order of their transient response; electric power, blower power, direct-injected fuel flow, and bulk fuel flow.

Appendix

A. Tables

Table 1 – Nominal SOFC operating condition.

Parameter	Nominal value
Net Power	3.5 kW
Stack Power	3.88 kW
Voltage	0.80 V
Cathode Inlet Temperature	994 K
Blower Power	0.38 kW

Table 2 – Disturbances, actuator and sensors applied to the linear model and control development.

Disturbances (D_i)	1) Fuel cell power
Actuators (A_i)	1) Cathode inlet temperature
	2) Blower power
Sensors (S_i)	1) Anode outlet temperature
	2) Plate temperature of 1st node
	3) Plate temperature of 2nd node
	4) Plate temperature of 3rd node
	5) Plate temperature of 5th node
	6) Plate temperature of 8th node
	7) Plate temperature of 10th node
	8) blower shaft speed
	9) Cathode outlet temperature
	10) Fuel flow rate
Control Variables (CV_i)	i) ith node electrolyte temperature

Table 3 – Nominal SOFC operating condition.

Parameter	Nominal value
Net Power	3.5 kW
Stack Power	3.685 kW
Voltage	0.80 V
Cathode Inlet Temperature	978 K
Blower Power	185.185

B. Performance Measure

Consider the following: $\dot{N}_{Nominal}$ is the required fuel flow rate at nominal condition, calculated proportional to current by using current based fuel control [13,32,49,50] as follows:

$$\dot{N}_{Nominal} = \frac{i*ncell}{U*2*F*1000*(X_{H_2} + X_{CO} + 4X_{CH_4})} \quad (B.1)$$

where the denominator includes the CH_4 injected directly plus the output of external reformer. Also, U is fuel utilization, for which a constant value is used, i is the current, F is Faraday constant, *n*cell is the number of cells, X_{H_2}, X_{CO}, X_{CH_4} are hydrogen, carbon monoxide and methane species concentrations, respectively. The total fuel flow rate is calculated based on the summation of $\dot{N}_{Nominal}$ plus $\Delta\dot{N}_{INT}$ in which $\Delta\dot{N}$ is the change in the flow rate of directly injected methane and can be calculated as

$$\Delta\dot{N}_{INT} = \frac{\Delta i * ncell}{U * 2 * F * 1000 * 4 * X_{CH_4}} \quad (B.2)$$

Where X_{CH_4} is 1/3 to maintain a steam to carbon ratio greater than 2:1. Net system power per mole CH_4 can be used as a measure of performance of fuel cell:

$$\text{Perf\_meas} = \frac{\text{Net power of system}}{\text{Flow rate of } CH_4} \quad (B.3)$$

$$\text{Flow rate of } CH_4 = (\text{Flow rate of } CH_4)_{INT} + (\text{Flow rate of } CH_4)_{EXT} \quad (B.4)$$

Recall net power is the power generated by fuel cell minus blower power demand and it is set to be the same for both cases of external reformation and partial internal reformation.

REFERENCES

[1] Murshed AM, Huang B, Nandakumar K. Estimation and control of solid oxide fuel cell system. Comput Chem Eng 2010;34(1):96–111.

[2] Tsai A, Banta L, Tucker D, Gemmen R. Multivariable robust control of a simulated hybrid solid oxide fuel cell Gas turbine plant. ASME J Fuel Cell Sci Tech 2010;7(4):041008.

[3] Fardadi M, Mueller F, Jabbari F. Feedback control of solid oxide fuel cell spatial temperature variation. J Power Sources 2010;195(13):4222–33.

[4] Fardadi M, McLarty D, Jabbari F. Actuator imperfections in spatial temperature control of SOFC. ASME J Fuel Cell Sci Technol June 2013;10:031005.

[5] Fardadi M. High performance control methods to reduce spatial temperature transients in emerging energy systems [Doctorate]. Irvine: University of California Irvine; 2013.

[6] Fardadi M., McLarty D., Jabbari F. Controlling spatial temperature variation in a rapid load following SOFC, ASME 2013 11th international conference on fuel cell Science, engineering.

[7] Pukrushpan TJ, Stefanopoulou GA, Huei P. In: Grimble JM, Johnson AM, editors. Control of fuel cell power systems: principles, modeling, analysis, and feedback design. London: Springer; 2005.

[8] Beckhaus P, Heinzel A, Mathiak J, Roes J. Dynamics of H_2 production by steam reforming. J Power Sources 2004;127(1–2):294–9.

[9] Gaynor R, Mueller F, Jabbari F, Brouwer J. On control concepts to prevent fuel starvation in solid oxide fuel cells. J Power Sources 2008;180(1):330–42.

[10] Ozgur Colpan C., Hamdullahpur F., Dincer F. Transient heat transfer modeling of a solid oxide fuel cell operating with humidified hydrogen. Proceedings of the international conference on hydrogen production, June 16–18, 2010, Istanbul, Turkey.

[11] Aguiar P, Adjiman CS, Brandon NP. Anode-supported intermediate temperature direct internal reforming solid oxide fuel cell. I: model-based steady-state performance. J Power Sources 15 November 2004;138(1–2):120–36.

[12] Aguiar P, Adjiman CS, Brandon NP. Anode-supported intermediate-temperature direct internal reforming solid oxide fuel cell: II. Model-based dynamic performance and control. J Power Sources 2005;147:136–47.

[13] Shaffer B, Brouwer J. Dynamic model for understanding spatial temperature and species distributions in internal-reforming solid oxide fuel cells. J Fuel Cell Sci Technol 2012;9(4):041012 [11 pages].

[14] Mueller F. The dynamics and control of integrated solid oxide fuel cell systems: transient load-following and fuel disturbance rejection [Doctorate]. Irvine: University of California, Irvine; 2008.

[15] Chalk S. American recovery and reinvestment act program plan for the office of energy efficiency and renewable energy: department of Energy. The Office of Energy Efficiency and Renewable Energy (EERE); 2009.

[16] Sison-Lebrilla E, Kibrya G, Tiangco V, Yen D, Sethi P, Kane M. Research development and demonstration roadmap. In: PIER renewable energy technologies program; 2007. Sacremento: California Energy Commission; August 2007. p. 45.

[17] Williams MC, Strakey JP, Surdoval WA, Wilson LC. Solid oxide fuel cell technology development in the U.S. Solid State Ionics 2006;177(19–25):2039–44.

[18] Haberman BA, Young JB. Numerical investigation of the air flow through a bundle of IP-SOFC modules. Int J Heat Mass Transf 2005;48(25–26):5475–87.

[19] Yang J, Li X, Mou H-G, Jian L. Predictive control of solid oxide fuel cell based on an improved Takagi-Sugeno fuzzy model. J Power Sources 2009;193(2):699–705.

[20] Yang J, Li X, Mou H-G, Jian L. Control-oriented thermal management of solid oxide fuel cells based on a modified Takagi-Sugeno fuzzy model. J Power Sources 2009;188(2):475–82.

[21] Nakajo A, Wuillemin Z, Van herle J, Favrat D. Simulation of thermal stresses in anode-supported solid oxide fuel cell stacks. Part I: probability of failure of the cells. J Power Sources 2009;193(1):203–15.

[22] Nakajo A, Wuillemin Z, Van herle J, Favrat D. Simulation of thermal stresses in anode-supported solid oxide fuel cell stacks. Part II: loss of gas-tightness, electrical contact and thermal buckling. J Power Sources 2009;193(1):216–26.

[23] Inui Y, Ito N, Nakajima T, Urata A. Analytical investigation on cell temperature control method of planar solid oxide fuel cell. Energy Convers Manag 2006;47(15–16):2319–28.

[24] Roberts R, Brouwer J, Jabbari F, Junker T, Ghezel-Ayagh H. Control design of an atmospheric solid oxide fuel cell/gas turbine hybrid system: variable versus fixed speed gas turbine operation. J Power Sources 2006;161(1):484–91.

[25] Serincan MF, Pasaogullari U, Sammes NM. A transient analysis of a micro-tubular solid oxide fuel cell (SOFC). J Power Sources 2009;194(2):864–72.

[26] Nakajo A, Stiller C, Harkegard G, Bolland O. Modeling of thermal stresses and probability of survival of tubular SOFC. J Power Sources 2006;158(1):287–94.

[27] Brouwer J, Jabbari F, Leal EM, Orr T. Analysis of a molten carbonate fuel cell: numerical modeling and experimental validation. J Power Sources 2006;158(1):213–24.

[28] Roberts R, Brouwer J. Dynamic simulation of a 220kW solid oxide fuel cell Gas turbine hybrid system with comparison to data. J Fuel Cell Sci Technol 2006;3(18):18–25.

[29] Kaneko T, Brouwer J, Samuelsen GS. Power and temperature control of fluctuating biomass gas... solid oxide fuel cell and micro Gas turbine hybrid system. J Power Sources 2006;160(1):316–25.

[30] Mueller F. Design and simulation of A Tubular solid oxide fuel cell system control strategy [Masters]. Irvine: University of California; 2005. p. 141.

[31] Roberts R. A dynamic fuel cell-gas turbine hybrid simulation methodology to establish control strategies and an improved balance of plant [Dissertation]. Irvine: University of California; 2005. p. 338.

[32] Roberts R, Brouwer J. Dynamic simulation of a pressurized 220 kW Solid oxide fuel-cell-Gas-turbine hybrid system: modeled performance compared to measured results. J Fuel Cell Sci Technol 2006;3(1):18–25.

[33] Mueller F, Jabbari F, Gaynor R, Brouwer J. Novel solid oxide fuel cell system controller for rapid load following. J Power Sources 2007;172(1):308–23.
[34] McLarty D. Thermodynamic modeling and dispatch of distributed Energy technologies including fuel cell – gas turbine hybrids [Doctorate]. Irvine: University of California, Irvine; 2013.
[35] Drescher I. Kinetik der Methan-Dampf-Refomierung [Ph.D. thesis]. Jülich, Jülich, Germany: Institut für Werkstoffe und Verfahren der Energietechnik, Forschungszentrums; 1999.
[36] Haberman BA, Young JB. Three-dimensional simulation of chemically reacting gas flows in the porous support structure of an integrated-planar solid oxide fuel cell. Int J Heat Mass Transf 2004;47:3617–29.
[37] Hedvig Paradis, Martin Andersson, Jinliang Yuan, Bengt Sundén. CFD modeling: different kinetic approaches for internal reforming reactions in anode supported SOFC. J Fuel Cell Sci Technol June 2011;8(3):031014 (Mar 01, 2011) (8 pages).
[38] Zhou K, Doyle JC. Essentials of robust control. Prentice Hall; 1998.
[39] Boyd S, Ghaoui LE, Feron E, Balakrishnan V. Linear matrix inequalities in system and control theory. 1994.
[40] Gahinet P, Apkarian P. A linear matrix inequality approach to H-infinity control. Int J Robust Nonlinear Control 1994;4(4):421–48.
[41] Scherer C, Gahinet P, Chilali M. Multiobjective output-feedback control via LMI optimization. IEEE Transact Automatic Control 1997;42(7):896–911.
[42] Skelton RE, Iwaskai T, Grigoriadis K. A unified algebraic approach to linear control design. London: Taylor and Francis; 1998.
[43] Mueller F, Jabbari F, Brouwer J, Roberts R, Junker T, Ghezel-Ayagh H. Control design for A bottoming solid oxide fuel cell Gas turbine hybrid system. J Fuel Cell Sci Technol 2007;4:221–30.
[44] Stiller C, Thorud B, Bolland O, Kandepu R, Imsland L. Control strategy for a solid oxide fuel cell and gas turbine hybrid system. J Power Sources 2006;158(1):303–15.
[45] Kandepu R, Imsland L, Foss BA, Stiller C, Thorud B, Bolland O. Modeling and control of a SOFC-GT-based autonomous power system. Energy 2007;32(4):406–17.
[46] Ferrari ML, Magistri L, Traverso A, Massardo AF. Control system for solid oxide fuel cell hybrid systems. Reno- Tahoe, Nevada, USA: ASME; June 6–9, 2005. p. 1–9.
[47] Ferrari ML, Traverso A, Magistri L, Massardo AF. Influence of the anodic recirculation transient behaviour on the SOFC hybrid system performance. J Power Sources 2005;149:22–32.
[48] Mogensen D, Grunwaldt J-D, Hendriksen PV, Dam-Johansen K, Nielsen JU. Internal steam reforming in solid oxide fuel cells: status and opportunities of kinetic studies and their impact on modelling. J Power Sources 1 January 2011;196(1):25–38.
[49] Kuniba Y. Development and analysis of load following SOFC/GT hybrid system control strategies for commercial building applications. Irvine: University of California, Irvine; 2007.
[50] Mueller F, Brouwer J, Jabbari F, Samuelsen GS. Dynamic simulation of an integrated solid oxide fuel cell system including current-based fuel flow control. ASME J Fuel Cell Sci Technol May, 2006;3(2):144–54.